Model Predictive Control for Integrated Photovoltaic (PV) and Electrolyser System ⋆

Ali Reza Pirouzfar, * **Sambeet Mishra,** * **Gaurav Mirlekar,** *
Koteswara Rao Putta **

* *Department of Electrical Engineering, Information Technology and Cybernetics, University of South-eastern Norway (USN), Porsgrunn 3918, Norway (e-mail: gaurav.mirlekar@usn.no).*
** *GCH2SOL AS, Trondheim 7028, Norway.*

Abstract: This paper investigates the integration of photovoltaic (PV) systems and proton exchange membrane (PEM) electrolysers to advance clean energy production and mitigate carbon emissions. The integration of PEM electrolysers with PV systems presents a promising solution for sustainable hydrogen production. This study utilizes Model Predictive Control (MPC) algorithms to manage the temperature of PEM electrolysers, crucial for enhancing performance and longevity. Temperature management is vital as lower temperatures increase overpotential, reducing efficiency, while higher temperatures improve performance but can accelerate membrane degradation. The paper simulates the PV-PEM electrolyser system using existing models to identify key parameters affecting system performance, employing MPC for efficient temperature regulation. The methodology involves modeling the integrated PV system, which includes Maximum Power Point Tracke (MPPT) algorithms, a DC-DC converter, and a PEM electrolyser. The MPPT algorithm ensures maximum power output from PV panels under varying irradiance levels, while buck-boost converters regulate voltage to meet electrolyser requirements. The electrolyser model considers mass and energy balance equations to understand the dynamics of hydrogen production and temperature control. Results from simulations indicate that the PV system's power generation is directly influenced by solar radiation and temperature. The study confirms that higher irradiance leads to greater power output, emphasizing the need for feasibility studies. The implementation of MPC algorithms demonstrates effective temperature control, ensuring stable operation and reduced membrane degradation. The integration of PV systems with PEM electrolysers, coupled with advanced control strategies like MPC, offers a viable pathway for enhancing renewable hydrogen production. This approach addresses the intermittency challenges of renewable energy sources and optimizes system performance.

Keywords: Advance process control, Process simulation, Renewable energy systems

1. INTRODUCTION

The transition to clean energy is critical for reducing fossil fuel dependence and minimizing carbon emissions. The International Energy Agency's annual outlook highlights various scenarios to address these challenges, notably the NetZero Emissions by 2050 pathway, which aims to stabilize global temperatures at 1.5°C and provide universal modern energy access by 2030 World Energy Outlook 2023. Central to this effort are photovoltaic (PV) systems and electrolysers, with solar PV projected to account for over half of new renewable power capacity by 2030 World Energy Outlook 2023. In 2022 alone, solar PV generation surged by 26% to 1293 TWh, underscoring its pivotal role in decarbonization World Energy Outlook 2023. In addition to solar energy, hydrogen-based fuels are considered a clean energy source for decarbonization. Hydrogen production methods include both fossil fuels and renewable sources. Conventional methods like steam reforming and coal gasification dominate current production, accounting for about 96% of the total Arsad et al. (2023) Hydrogen forecast to 2050. Renewable-based methods, particularly electrolysis, are gaining traction due to their clean energy potential Arsad et al. (2023). Proton Exchange Membrane (PEM) and Alkaline electrolysers are the most efficient and commercially available technologies Hydrogen forecast to 2050. Integrating PEM electrolysers with photovoltaic (PV) systems presents a promising solution for reducing emissions and achieving sustainability. However, electrolysers currently contribute only 4% to hydrogen production from renewable energies, primarily due to their higher average costs. Forecasts from DNV Hydrogen forecast to 2050 suggest that the average costs of electrolysers are expected to decrease by 25% by 2030 and by 50% by 2050,

⋆ We gratefully acknowledge the financial support from the Department of Electrical Engineering, Information Technology and Cybernetics at the University of South-eastern Norway (USN). corresponding author's e-mail: gaurav.mirlekar@usn.no

based on current market insights. Water electrolysis stands as a leading industrial method for producing nearly pure hydrogen, highlighting its future significance. Moreover, electrolysers play a pivotal role in converting energy into gas within Power-to-Gas (P2G) systems, which transform renewable energy sources such as wind, solar, geothermal, and hydro into gas. Although currently underutilized, this approach is projected to grow significantly, with hydrogen production via electrolysis expected to reach 22% by 2050Arsad et al. (2023).

Renewable energy sources, however, face intermittency challenges due to varying climatic conditions. This instability necessitates auxiliary energy systems to ensure consistent hydrogen production, as electrolysers require a minimum current density for safe operation Afshari et al. (2021). A grid-connected setup, leveraging Maximum Power Point Tracker (MPPT) controllers, can optimize power from PV panels to electrolysers Gutiérrez-Martín et al. (2024). Enhancing system performance further, buck-boost converters can regulate voltage from PV arrays to meet electrolyser requirements Ruuskanen et al. (2020). In this study, the simulation of PEM electrolysers is conducted using existing models Abdin et al. (2015), Marangio et al. (2009), Cavaliere (2023), and Falcão and Pinto (2020) to identify and analyze the key parameters affecting the system.

Furthermore, Model Predictive Control (MPC), offer efficient temperature management, critical for enhancing system performance and longevity Scheepers et al. (2021) Majumdar et al. (2023). Simplified control models, like those using piece-wise affine and multi-parametric approaches, have shown promise in minimizing hydrogen production costs and managing operational constraints Flamm et al. (2021) Ogumerem and Pistikopoulos (2020). This paper utilizes an energy balance equation and a state-space model for temperature control in PEM water electrolysers, adapting MPC techniques for improved efficiency. It has been done by regulating water flow rate in to the system as the manipulating variable to stable the cell temperature and leads lower membrane degradation of the PEM electrolyser.

2. PROCESS DESCRIPTION

The objective of this study is to model a PV system, incorporating MPPT algorithms, a DC-DC converter, and a PEM electrolyser, and to apply model predictive control (MPC) algorithms to manage the electrolyser's temperature. As illustrated in Fig.1, electricity generated by photovoltaic panels is regulated by DC-DC converters, primarily buck-boost types, to stabilize the output current, which is then supplied to the PEM electrolyser. This process splits water into hydrogen and oxygen, which are collected in separate containers for drying and further use or storage. MPC are crucial due to the operational conditions of the electrolysers. PEM electrolysers typically operate at temperatures between 60-90°C and pressures around 30 bar Arsad et al. (2023). In terms of temperature of the electrolyser, lower temperatures increase overpotential, reducing efficiency, while higher temperatures enhance performance by improving membrane ionic conductivity and reaction kinetics, thus reducing overpotentials Cavaliere (2023).

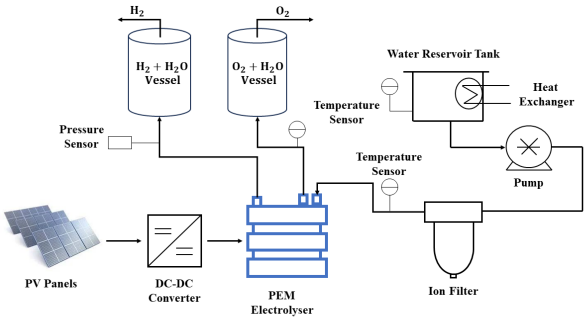

Fig. 1. Process schematic of integrated PV and PEM Electrolyser System.

However, higher temperatures can accelerate the degradation of polymer membranes, primarily due to thermal, chemical, and mechanical stresses, leading to thinning, unzipping, loss of functional groups, or membrane rupture Babic et al. (2017). Monitoring and controlling the temperature is therefore essential to prevent degradation and maintain efficiency.

The increase in electrolyser temperature results from endothermic reactions during water electrolysis and Joule heating, where electric current generates heat as it passes through the conductor Ogumerem and Pistikopoulos (2020). Sudden increases in hydrogen production can raise temperatures, affecting membrane stability and lifespan. Typical methods to maintain the desired temperature range include cooling airflow or adjusting the cooling water flow rate. In the system depicted in Fig.1, a water reservoir, temperature sensor, and heat exchanger keeps the water temperature constant. Water is pumped through an ion filter to reduce resistance and manage flow rates before being directed to the electrolyser. Temperature sensors at the inlet and outlet monitor changes. MPC algorithms, based on Ogumerem and Pistikopoulos (2020), control temperature fluctuations by adjusting the water flow rate, acting as a coolant. The manipulated variable is the water flow rate, and the state variable is the temperature derived from the energy balance equation. The MPC algorithms are based on a linear state-space model derived from solving the energy balance and mass balance equations for each part of the electrolyser, simplifying system modeling.

3. METHODOLOGY

Mathematical modeling and governing equation of the integrated system including photovoltaic (PV) system with MPPT, DC-DC converter, PEM electrolyser and MPC algorithms has been presented in this section.

3.1 Photovoltaic system

In PV systems solar radiation, containing photons, excites electrons upon contact with PV panels, creating a P-N junction in semiconductors and generating current. The more photons that hit the PV panels, the greater the current produced. Therefore, irradiance information based on the system's location is critical for calculations. Fig. 2 demonstrates, the irradiance data for the University of South-East Norway (USN) in Porsgrunn, Norway (latitude 59.138, longitude 9.672) for June 2020.

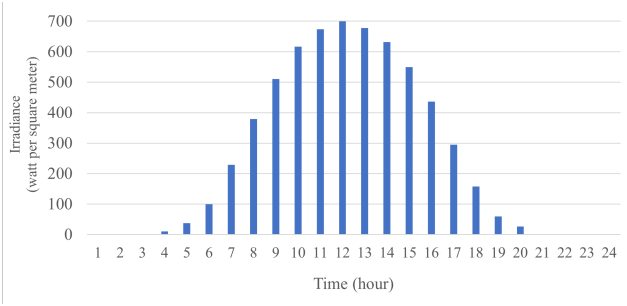

Fig. 2. Hourly solar irradiance $\frac{W}{m^2}$.

3.2 Modeling of photovoltaic Modules

The current voltage equation for modeling the PV system can be represented as follows:

$$I_{pv} = I_{ph} - I_0 \left[\exp\left(q\frac{V_{pv} + I_{pv} \cdot R_s}{AKT_j}\right) - 1\right] \quad (1)$$

$$I_{ph} = I_{ph\_G} \cdot (1 + \alpha_{sc} \cdot \Delta T) \quad (2)$$

$$I_{ph\_G} = I_{sc} \cdot \left(\frac{G}{G_{ref}}\right) \quad (3)$$

$$\Delta T = T_j - T_{j\_ref} \quad (4)$$

In which, I_{pv}(A) is the photovoltaic current, I_{ph} (A) is the photo-current, I_0 (A) is the reverse saturation current of the diode, q is the electron charge which is equal to 1.602×10^{-19} (C), K is the Botzman's constant which is equal to $1.381 \times 10^{-23}(\frac{J}{K})$, A is diode ideality factor, T_j is junction temperature of the panels (°)K, R_s is series of resistance and V_{pv} is the voltage across PV cell (V). Also in the Eq.2 to Eq.4, I_{ph_G} represent current depending on short circuit current, reference irradiance of $G_{ref} = 1000$ $\frac{W}{m^2}$ and reference temperature of $T_{j\_ref} = 25°C$. Also α_{sc} is the temperature coefficient of short-current ($°K$) found on the datasheet. For finding reverse saturation current at any temperature (I_0), the Eq.5 can be obtained as follow:

$$I_0 = \frac{I_{sc}}{\left[\exp\left(\frac{V_{oc}}{V_{th\_T_{j\_ref}}}\right) - 1\right]} \cdot \left[\exp\left(\frac{-q \cdot \frac{E_g}{AK}}{\frac{1}{T_j} - \frac{1}{T_{j\_ref}}}\right)\right] \cdot \left(\frac{T_j}{T_{j\_ref}}\right)^{\frac{3}{A}} \quad (5)$$

In which E_g represents the band gap energy considered as 1.12 electron volt (eV)Chander et al. (2015). So by substituting Eqs. 2 and 5 in the Eq.1, the final photovoltaic current is obtained. Also in order to find R_s in the Eq.1, term "-1" added to the exponential equation:

$$R_s = -\frac{dV_{pv}}{dI_{pv}}\Big|_{V_{pv}=V_{oc}} - \frac{1}{W} \quad (6)$$

and:

$$W = q \cdot \frac{I_{sc}}{AKT_j} \quad (7)$$

The term of $-\frac{dV_{pv}}{dI_{pv}}$, obtained by experiment or by $I_{pv} - V_{pv}$characteristic of the manufacturer mentioned on datasheets. Also, for solving Eq.1, Newton's method has been used.

3.3 Maximum Power Point Tracker algorithm

According to Afshari et al. (2021), maintaining minimum current density levels is crucial for safety at varying pressures, as hydrogen concentration decreases relative to oxygen at the anode at lower current densities. To address this, the Maximum Power Point Tracking (MPPT) algorithm ensures maximum power output from PV panels under different irradiance levels. As defined by Zhou et al. (2010), MPPT, combined with a DC-DC converter, allows a photovoltaic generator to produce optimal power consistently, regardless of changes in irradiance and temperature, by operating at the optimal voltage and current (V_{opt}, I_{opt}). Various MPPT algorithms exist, with the Perturb and Observe (P&O) method being used in this study. The P&O method iteratively seeks the maximum power point by continuously evaluating the PV module's current and voltage. The MPPT algorithm based on the P&O method illustrates how the algorithm identifies the maximum power point and corresponding voltage under different hourly irradiance conditions. This algorithm is repeated for each hourly irradiance to maximize the daily power output.

3.4 DC-DC converters

The governing equation of the DC-DC converter is presented. Three main types of converters—boost, buck, and buck-boost—are commonly employed in integrated photovoltaic and electrolyser systems to adjust the final voltage. Average modeling methods are typically utilized for simulating these converters. Ruuskanen et al. (2020) highlights that current ripple reduces the efficiency of alkaline electrolyzers, necessitating better power electronics control, potentially applicable to PEM electrolyzers as well. Energy suppliers using photovoltaic systems and batteries require DC-DC converters to adjust voltage and current levels, as these converters are essential for modifying electrical voltage levels between generators and loads Mohan (2012). Simulations show that solar power output and voltage fluctuate throughout the day due to irradiance changes, while electrolyzers require a steady 320V. Buck-Boost converters adjust output voltage above or below the input based on the switch duty ratio D. The output voltage of a Buck-Boost converter, determined by the duty cycle D, is given by $\frac{V_{out}}{V_{in}} = \frac{D}{1-D}$ Hart (2011). With $D > 0.5$, it operates as a boost converter; with $D < 0.5$, as a buck converter. This hybrid model combines boost behavior when the IGBT is on and buck behavior when off. By implementing average model methodologies, the final model representing the converter is given by the following equations:

$$\frac{di_L}{dt} = \frac{1}{L}\left(DV_{in} - (1-D)v_C\right) \quad (8)$$

$$\frac{dv_C}{dt} = \frac{1}{C}\left((1-D)i_L - \frac{v_C}{R}\right) \quad (9)$$

3.5 Modeling of electrolyser system

The electrolyser cell consists of a pair of conductive electrodes immersed in an electrolyte that facilitates ionic conduction. Upon the application of voltage across these electrodes, oxidative processes occur at the anode, while reduction reactions occur at the cathode. The anode and cathode are connected through the flow of current. In this study, PEM electrolyser model is employed for simulation purposes. A detailed explanation of operating characteristics of PEM electrolysers presented in Table.1. To accurately determine the total voltage of an electrolyzer, it is essential to understand the governing equations derived

from the mass balance in each part of the electrolyzer (Rabascall and Mirlekar (2023)). Accordingly, three control volumes have been defined within the electrolyzer, including the anode, cathode, and membrane sections. The overall water flow across the membrane can be described through three processes: diffusion, electro-osmotic drag, and hydraulic pressure effects representing membrane mass transfer dynamics. Additionally, energy balance equation is chosen from the literature to represent electrolyser temperature (Ogumerem and Pistikopoulos (2020)).

Table 1. Standard Characteristics of Polymer Electrolyte Membrane (PEM).

PEM electrolyser characteristics			
Technology maturity	Commercial	Anode	IrO_2, RuO_2
Electrolyte	Polymer (Solid)	Cathode	Pt, Pt-Pd
Cell temperature, °C	60 - 90	System energy consumption, kWh/Nm^3	4.5 - 7.0
Operating Pressure (bar)	15 - 30	H_2 Capacity (Nm^3/h)	<40
Cell Voltage (V)	1.8 - 2.2	H_2 purity	99.9
Current Density (A/cm^2)	0.6 - 2	Stack lifetime, hr	<20,000
Power density (W/cm^2)	Up to 4.4	System lifetime, yr	10 - 20
Voltage Efficiency (%)	67 - 82	Charge carrier	H^+

The anode mass transfer module computes the flows of oxygen and water, as well as their respective partial pressures. At the anode, water undergoes oxidation to yield oxygen, electrons, and protons. The cathode mass transfer dynamics module computes the partial pressures and flow rates of hydrogen and water at the cathode, where protons undergo reduction. The objective of these calculations is to determine the partial pressures of each species at both the cathode and anode sides. It is essential to note that the calculated partial pressures are utilized in subsequent calculations to determine the total potential of the electrolyzer and the energy balance equation.

3.6 Model predictive control

We utilize a derived model based on the energy balance of the electrolyser, as discussed in previous section. This model captures the temperature dynamics of the electrolyser and can be manipulated by adjusting the water flow rate into the system. In MPC, the process of forecasting future states and outputs, formulating, and solving an optimization problem is iterated at each time step. This iterative approach, known as a sliding horizon strategy, ensures continuous feedback and control adaptation. A linear state space model has been employed for MPC algorithms. A brief description of the linear state space model presented as follow. The general form of linear state space model can be written as,

$$x_{k+1} = Ax_k + Bu_k + v_k \rightarrow \quad \text{State equation} \tag{10}$$

$$y_k = Cx_k + Du_k + w_k \rightarrow \text{Measurment equation} \tag{11}$$

Here, A, B, C, and D represent system matrices. $A \in R^{n_x \times n_x}$, $B \in R^{n_x \times n_u}$, $C \in R^{n_y \times n_x}$, and $D \in R^{n_y \times n_u}$. Additionally, $v_k \in R^{n_x}$ and $w_k \in R^{n_y}$ are zero-mean random variables with specific variances. v_k represents process noise, while w_k denotes measurement noise. It is assumed that v_k and w_k are uncorrelated (stochastically independent), i.e., $\text{corr}[v_k,\ w_j] = 0$ for all k and j. This implies that random disturbances affecting measurements are unrelated to the randomness in the system states or processes themselves.

For designing linear MPC, the nonlinear derived model is linearized to obtain a continuous time linear state space model, that is, the derivation of energy balance balance equation on PEM electrolyser has been implemented. It is important to note that the MPC algorithm has been implemeted on electrolyser to control operating temperature based on the energy balance equation as follows:

$$c_p M \frac{dT}{dt} = n_{cell} I(V_{oc} - V_0) + \dot{M}^{an}_{H_2O,in} c_{p_{H_2O}} (T - T^{an}_{in}) - H_{rad} \tag{12}$$

Where c_p is the specific heat capacity (J/kg.K), V_0 is the thermoneutral voltage expressed as a function of temperature anode pressure and H_{rad} is the the heat loss from radiation.

Finally, MPC is designed using the discrete time linear state space model. The initial step in linearizing a nonlinear model involves establishing an equilibrium point to derive a linear model around it. It is assumed that the actual system dynamics approximate the nominal trajectories, that is, they are near the defined operating points. Also the cost function can be used in order to implement the optimization. So:

$$\min_u J = \sum_{k=1}^{N-1} \left((y_k - y_k^R)^T Q R (y_k - y_k^R) \right) + \sum_{k=0}^{M-1} (\Delta u_k^T R \Delta u_k) \tag{13}$$

By understanding the MPC concepts and fundamentals, the implementation of this algorithms on integrated system has been done in Simulink by use of MPC block. While the mpcDesigner command used to set the mentioned values for the model. Finally, the MPC block used with the designed plant of electrolyser to set the temperature at the set point value. It is also of the essence to mention that the reference value for the electrolyser operating point considered as 63°C while weighting matrices in the MPC controller considered on the error between the actual altitude and the target to be in the range of 5°C and positive water flow rate based on the pump operation.

4. SIMULATION RESULTS

In this section simulation results of an integrated dynamic system, encompassing photovoltaic panels with an MPPT algorithm, a DC-DC converter, a PEM electrolyser, and MPC implementation are presented.

4.1 Photovoltaic system simulation results

Power generation is directly influenced by solar radiation as discussed in Sections 2 and 3. The solar irradiance is illustrated in Fig. 2. Additionally, temperature affects the current-voltage produced by the PV system, with a standardized temperature of 25°C assumed for all simulations. Fig. 3 illustrates the current-voltage and power-voltage diagrams at a different radiation levels and a temperature of 25°C, based on MATLAB mathematical simulations. As depicted in Fig. 3, the maximum power output of the PV system is approximately 200 watts, aligning with

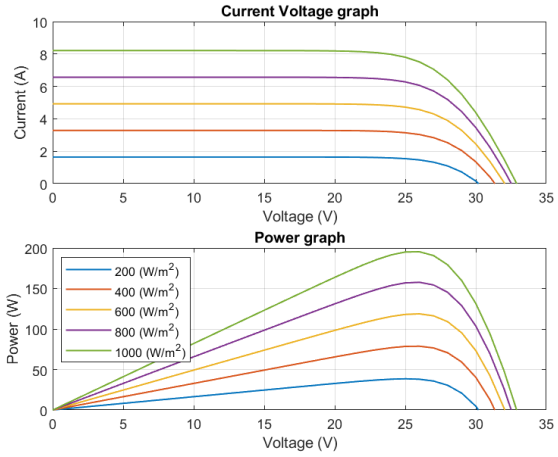

Fig. 3. Current-voltage and power-voltage simulation of photovoltaic panel.

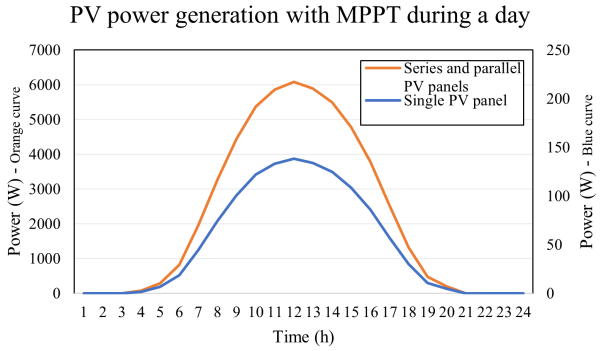

Fig. 4. Simulation of PV system's power during a day.

the findings of Ma et al. (2013) under similar conditions of 1000 ($\frac{W}{m^2}$) and a temperature of 25(°)C. The behavior of these curves closely mirrors those presented in the cited study. Due to the inherent characteristics of photovoltaic systems, the current-voltage and power-voltage profiles vary with different levels of irradiance. It is typical for manufacturers to display these curves at various standard irradiances such as 200, 400, 600, 800, and 1000 ($\frac{W}{m^2}$). The KC200GT PV module, utilized in the study by Ma et al. (2013), demonstrates how PV characteristics are impacted under various irradiance levels, maintaining a constant temperature of 25°C. Fig.3 shows that the behavior of these curves is consistent with those found in PV paneldatasheet [1], further validating the model's accuracy.

As shown in Fig. 3, higher solar irradiance results in greater power output from photovoltaic panels due to increased photon absorption. As this study primarily focuses on the electrolyser and the implementation of MPC algorithms for temperature control, the photovoltaic system is treated solely as a renewable energy source, with simulation and modeling efforts emphasizing accurate representation and validation against existing literature.

From Fig. 3, it is evident that the system yields maximum power output around 25 volts per radiation level. To achieve this maximum power, the Maximum Power Point

[1] https://www.energymatters.com.au/images/kyocera/KC200GT.pdf

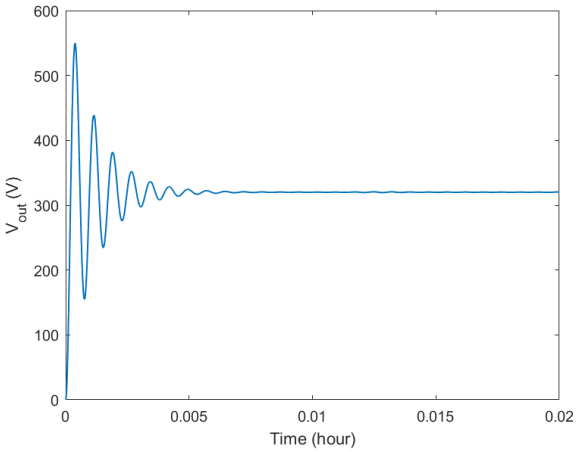

Fig. 5. Simulation of buck-boost converter with output voltage of 320(V).

algorithm is integrated into the PV system, ensuring that the output is optimized for peak power generation. Simulation of the system over 24 hours, based on hourly irradiance data (Fig. 2), reveals a correlation between power production and irradiance fluctuations, as shown in Fig. 4. However, since the location lacks a radiation level of 1000 $\frac{W}{m^2}$, the system operates below its maximum potential, peaking at approximately 148 W at noon.

The power generated by the PV system needs to be transmitted to the electrolyser to meet the energy demand. This necessitates the use of a DC-DC converter to regulate the fluctuating power output from the PV panels, ensuring stable energy supply to the system.

4.2 DC-DC converter simulation results

The simulations of buck-boost converters are conducted to validate the methodology employed in this study against existing literature. A buck-boost converter, ideal for renewable energy systems with inherent power fluctuations, ensures a stable 320-volt supply to the electrolyser, as demonstrated in simulations based on Eqs. 8 and 9, is depicted in Fig. 5. The design parameters, including inductor, resistor, and capacitor values are calculated accordingly to achieve desired output voltage, operating at the lowest irradiance. This was accomplished with a frequency of 20kHz and a voltage deviation of $\Delta V_{out} = 0.05 \cdot V_{in}$ to reach the final voltage of 320V. The decision to design the buck-boost converter to achieve an output voltage of 320 volts was driven primarily by the need to align with grid specifications (for the scenarios where can be combined PV system with the grid), particularly the root mean square voltage typical in many grid systems. This voltage level ensures that the power produced by the PV system is compatible with the grid infrastructure, facilitating a seamless integration of the renewable energy source with the existing power network. Ensuring compatibility with the grid voltage is crucial for efficient energy transfer, minimizing losses, and ensuring stability in the power system, which ultimately enhances the reliability and effectiveness of both the renewable integration and the grid operation.

The simulation of a single input voltage from the PV panels is shown in Fig. 5. We now proceed to depict the

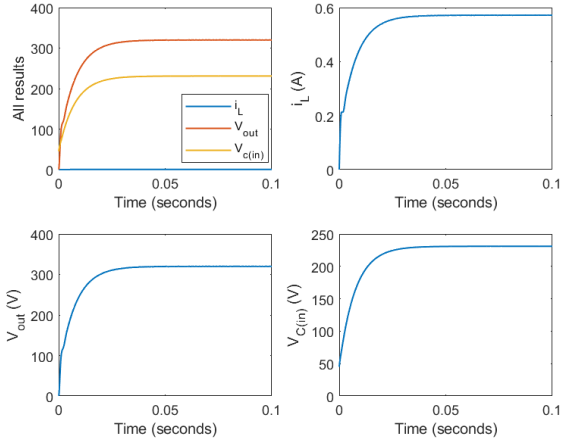

Fig. 6. Simulation of buck-boost converter with an inlet capacitor.

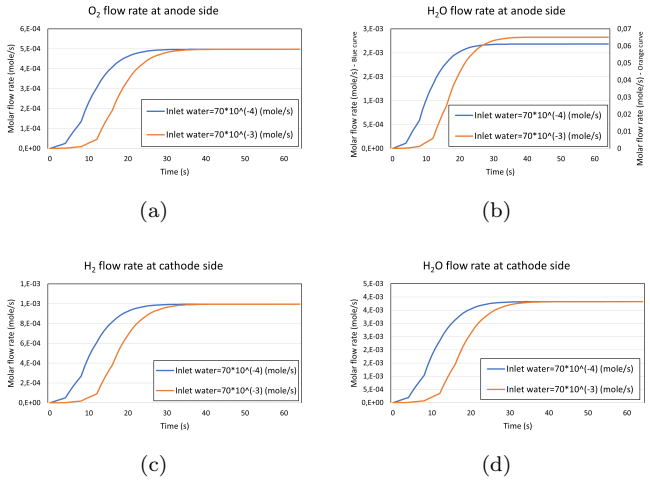

Fig. 7. Hydrogen, oxygen and water produced flow rate from cathode and anode part of electrolyser with different inlet water flow rate.

the comprehensive simulation and modeling of a DC-DC converter, which adjusts various hourly changing voltage ar-rays from the PV panels to a desired voltage level. It is crucial to highlight that in this mathematical simulation, the duty cycle is adjusted on an hourly basis in response to changes in solar radiation. This adjustment ensures that the output voltage from the PV system aligns with the required 320V for the DC bus. Adjustments in the duty cycle are managed by an appropriate controller within the circuit, as discussed in Safari and Mekhilef (2010). Over-shooting fluctuations can be mitigated by integrating a capacitor at the input of the buck-boost converter circuit. This capacitor functions by storing excess voltage and charging, thus smoothing out the overshoots in the circuit. Xiao (2017) have provided models that demonstrate this effect. Implementation of these models shows that initial fluctuations are effectively eliminated from the system, as illustrated in Fig.6 under the same conditions mentioned in Fig.5.

4.3 Electrolyser simulation results

The simulation results of the PEM electrolyser are presented in the following section. Figure 7 presents the simulation modeling results of the different water flow rate into the cathode side of the electrolyser. Notably, increasing the water flow rate does not enhance hydrogen production, which is primarily dependent on the amount of electric current supplied to the electrolyser. According to Ogumerem and Pistikopoulos (2020), increasing the current flow directly boosts hydrogen output. While the water flow rate may not influence hydrogen production, as illustrated in Figure 7, it plays a critical role in cooling the electrolyser. Figure 7 uses water flow rates of 70×10^{-4} and 70×10^{-3} moles per second for comparison. The analysis shows that hydrogen production remains unaffected by changes in the water flow rate but is expected to increase with higher current. Additionally, the study indicates that a water flow rate below 50×10^{-4} mole per second can lead to abnormal outcomes, such as negative water production at the anode with simulated specifications. The system also can be faced with upper limits on the water flow rate due to the capacities of the pump and ion filter components.

Temperature and pressure significantly influence electrolyser performance, making their accurate measurement and control crucial for effective system modeling. To accurately model these systems, it is essential to understand the pressures at the anode and cathode, which influence several critical parameters. Additionally, the differential pressure (ΔP) across the membrane (used for pressure effect based on the Darcy's law) is fundamental for accurately predicting water transport through it. The dependency of the electro-osmotic drag coefficient (n_d) on pressure underscores the complexity of electrolyser dynamics under varying operational pressures. The thermal sensitivity of the electrolyser also poses significant challenges. Fluctuations in temperature can compromise membrane integrity and, in extreme cases, could lead to hazardous conditions if hydrogen and oxygen mix explosively. This study, therefore, adheres to operating temperatures for PEM electrolysers typically between 60°C and 90°C with the pressure of 30 bar, aligning with industry standards to minimize risks and optimize performance. The membrane, assumed fully hydrated, exhibits conductivity solely dependent on temperature. The polarisation curve comprises various potentials, including V_{oc}, V_{act}, V_{con}, and V_{ohm}. The contribution of each potential to the polarisation curve is depicted in Fig. 8. Simulations conducted at a symmetric pressure of 1 bar for the cell demonstrate that higher temperatures correlate with reduced overpotential in the electrolyser (Fig. 9(a)). Conversely, as depicted in Fig. 9(b), maintaining a constant temperature of 60°C while increasing pressure leads to heightened overpotential in the electrolyser. Understanding these dynamics is essential for optimizing electrolyser performance and guiding design decisions.

4.4 Model predictive control implementation results

The system description of the PEM electrolyser has been elucidated thus far. Modeling is a crucial precursor to implementing advanced control systems like MPC algorithms, as they rely heavily on accurate simulation models.

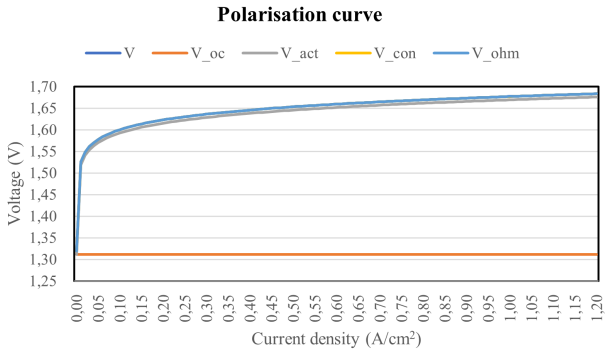

Fig. 8. Share of each potential to the final polarisation curve of the PEM electrolyser.

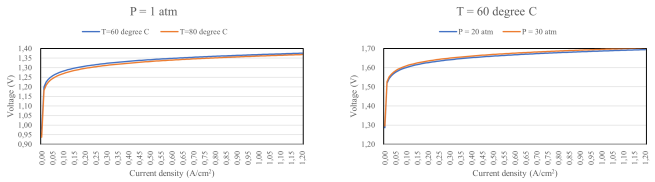

(a) Influence of cell temperature. (b) Influence of cell pressure.

Fig. 9. Influence of cell temperature and pressure on the electrolyser.

Commencing with MPC algorithms, as discussed in Section 3.6, it is crucial to comprehend the model governing the system, derived from the energy balance equation elucidated by Ogumerem and Pistikopoulos (2020). To maintain consistency with the referenced study, a linear state-space form was chosen. To determine matrices A and B, it is essential to derive the derivation form of the energy balance formula based on the states and control variables. The state variable considered as the temperature in the Eq.12 while the control variable is the water flow rate into the system by which the cell temperature can be controlled. This involves selecting state, control, and output parameters, with the electrolyser temperature chosen as the state variable to be controlled by the water flow rate. Additionally, the temperature difference from the set point temperature could serve as the output variable. Choosing an operating point around 60°C for the electrolyser facilitates the derivation of A and B matrices as follows which will be gain as the derivation form of Eq.12 based on state variable wich is temperature and control variable that is water flow rate effecting in reducing cell temperature with following equation form:

$$A = \left[\frac{\left(\frac{d(n_{cell} I(V_{oc} - V_0) + \dot{M}^{an}_{H_2O,in} c_{p_{H_2O}} (T - T^{an}_{in}) - H_{rad})}{dT} \right)}{C_p M_{H_2O}} \right] \quad (14)$$

$$B = \left[\frac{\left(\frac{d(n_{cell} I(V_{oc} - V_0) + \dot{M}^{an}_{H_2O,in} c_{p_{H_2O}} (T - T^{an}_{in}) - H_{rad})}{d\dot{M}^{an}_{H_2O,in}} \right)}{C_p M_{H_2O}} \right] \quad (15)$$

To determine the A matrix, it is essential to define the control operating point. This parameter can be determined by setting the energy balance equation to zero and substituting the set temperature of the operating point.

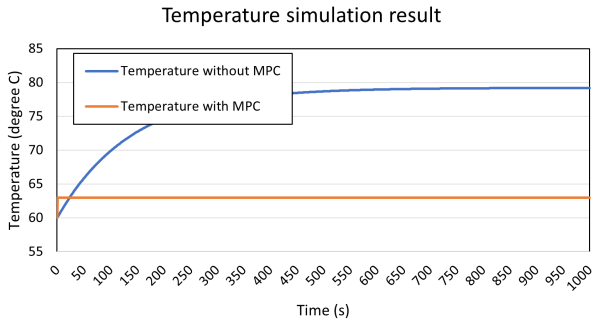

Fig. 10. Simulink result of simulated energy balance model of the PEM electrolyser.

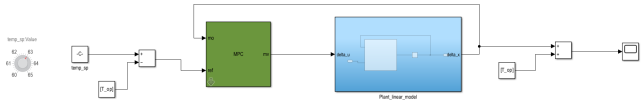

Fig. 11. MPC block implementation in Simulink.

$$\dot{M}^{an}_{H_2O,in} = \frac{1}{c_{p_{H_2O}} (T_{op} - T^{an}_{in})} (-n_{cell} I(V_{oc} - V_0) + H_{rad}) \quad (16)$$

To simulate the model in state space form, a sampling time of 0.1 seconds was specified, and the system was named 'plant' using the 'ss' function in MATLAB. Additionally, the model was discretized using the 'c2d' function. Following the implementation of the state space model, simulation was conducted using the Simulink environment in MATLAB. Fig. 10 highlights the need for implementing MPC algorithms to regulate the setpoint temperature within the range of 60-65°C. To achieve this, the MPC block was integrated into the Simulink diagram alongside the designed system labeled 'plant.' Fig. 11 illustrates the schematic of the interconnected blocks within the Simulink environment, including the MPC block.

In Fig. 11, the output of the simulation generated by the linear state space model is fed back to the MPC block for comparison with the predetermined reference setpoint. This feedback loop enables the system to dynamically adjust the flow rate to regulate the temperature at the desired value. Expanding upon this concept, the MPC block continuously receives feedback from the simulation results and compares it with the target setpoint temperature of 63°C. By analyzing this feedback, the MPC algorithm calculates the necessary adjustments to the control inputs, ensuring that the system maintains the temperature within the specified range. Moreover, the simulation output, depicted in Fig.10, provides a visual representation of how effectively the MPC algorithm controls the system. It showcases the temperature response over time, demonstrating the system's ability to track and stabilize the temperature around the desired setpoint. Utilizing the 'mpcDesigner' tool in the MATLAB workspace enables users to configure and fine-tune the controller settings effectively. In summary, the simulation results encapsulated in the series of figures, indicate successful temperature regulation by the MPC algorithm. This was achieved through system modeling, controller design, and feedback mecha-

nisms that adjust the flow rate to stabilize temperature. The results validate the robustness and precision of the designed MPC system in achieving and maintaining the desired operational conditions within the electrolyser.

5. CONCLUSIONS

The study reviewed extensive literature on hydrogen production, particularly focusing on solar-powered proton exchange membrane (PEM) electrolysers, which were identified as effective but requiring stable operation. Model Predictive Control (MPC) was chosen for its capability to regulate electrolyser temperature, enhancing operational efficiency. Simulations were performed for integrated system, including photovoltaic (PV) panels and PEM electrolysers. MPC was tested, proving successful in maintaining desired electrolyser temperatures. The system incorporated Maximum Power Point Tracking (MPPT) to optimize power output from PV panels, and DC-DC converters were evaluated, with the buck-boost converter providing stable power adjustments suitable for renewable energies. The simulations, which also considered various operational parameters, demonstrated the potential for high efficiency and detailed system behavior under varying conditions. The study achieved successful system modeling and simulation, demonstrating a stable adjustment time that was approximately 10 minutes faster to the selected set point with MPC algorithms compared to without. Additionally, the findings suggest that more detailed models are necessary for practical application and scaling up the project.

REFERENCES

Abdin, Z., Webb, C., and Gray, E.M. (2015). Modelling and simulation of a proton exchange membrane (pem) electrolyser cell. *International journal of hydrogen energy*, 40(39), 13243–13257.

Afshari, E., Khodabakhsh, S., Jahantigh, N., and Toghyani, S. (2021). Performance assessment of gas crossover phenomenon and water transport mechanism in high pressure pem electrolyzer. *International Journal of Hydrogen Energy*, 46(19), 11029–11040.

Arsad, A., Hannan, M., Al-Shetwi, A.Q., Begum, R., Hossain, M., Ker, P.J., and Mahlia, T.I. (2023). Hydrogen electrolyser technologies and their modelling for sustainable energy production: a comprehensive review and suggestions. *International Journal of Hydrogen Energy*.

Babic, U., Suermann, M., Büchi, F.N., Gubler, L., and Schmidt, T.J. (2017). Critical review—identifying critical gaps for polymer electrolyte water electrolysis development. *Journal of The Electrochemical Society*, 164(4), F387.

Cavaliere, P. (2023). *Water Electrolysis for Hydrogen Production*. Springer Nature Switzerland AG, Gewerbestrasse 11, 6330 Cham, Switzerland.

Chander, S., Purohit, A., Nehra, A., Nehra, S., and Dhaka, M. (2015). A study on spectral response and external quantum efficiency of mono-crystalline silicon solar cell. *International journal of renewable energy research*, 5(1), 41–44.

Falcão, D. and Pinto, A. (2020). A review on pem electrolyzer modelling: Guidelines for beginners. *Journal of cleaner production*, 261, 121184.

uchi, F.N., and Lygeros, J. (2021). Electrolyzer modeling and real-time control for optimized production of hydrogen gas. *Applied Energy*, 281, 116031.

Gutiérrez-Martín, F., Díaz-López, J., Caravaca, A., and Dos Santos-García, A. (2024). Modeling and simulation of integrated solar pv-hydrogen systems. *International Journal of Hydrogen Energy*, 52, 995–1006.

Hart, D.W. (2011). Power electronics–dc-dc converter. *Valparaiso University, Valparaiso, Indiana*, 2, 198–205.

Hydrogen forecast to 2050 (2022). Hydrogen forecast to 2050. https://www.dnv.com/focus-areas/hydrogen/forecast-to-2050.html. Accessed on 15 Jan 2024.

Ma, J., Man, K.L., Ting, T., Zhang, N., Guan, S.U., Wong, P.W., et al. (2013). Approximate single-diode photovoltaic model for efficient i-v characteristics estimation. *The Scientific World Journal*, 2013.

Majumdar, A., Haas, M., Elliot, I., and Nazari, S. (2023). Control and control-oriented modeling of pem water electrolyzers: A review. *International Journal of Hydrogen Energy*.

Marangio, F., Santarelli, M., and Calì, M. (2009). Theoretical model and experimental analysis of a high pressure pem water electrolyser for hydrogen production. *International journal of hydrogen energy*, 34(3), 1143–1158.

Mohan, N. (2012). *Power electronics: a first course*. John Wiley & Sons.

Ogumerem, G.S. and Pistikopoulos, E.N. (2020). Parametric optimization and control for a smart proton exchange membrane water electrolysis (pemwe) system. *Journal of Process Control*, 91, 37–49.

Rabascall, J.B. and Mirlekar, G. (2023). Sustainability analysis and simulation of a polymer electrolyte membrane (pem) electrolyser for green hydrogen production. In *Proceedings of the 64th International Conference of Scandinavian Simulation Society, SIMS 2023 Västerås, Sweden, September 25-28, 2023*, 110–117.

Ruuskanen, V., Koponen, J., Kosonen, A., Niemelä, M., Ahola, J., and Häm¨

and reactive power of water electrolyzers supplied with thyristor converters. *Journal of Power Sources*, 459, 228075.

Safari, A. and Mekhilef, S. (2010). Simulation and hardware implementation of incremental conductance mppt with direct control method using cuk converter. *IEEE transactions on industrial electronics*, 58(4), 1154–1161.

uller, M., Carmo, M., and Lehnert, W. (2021). Temperature optimization for improving polymer electrolyte membrane-water electrolysis system efficiency. *Applied Energy*, 283, 116270.

World Energy Outlook 2023 (2023). World Energy Outlook 2023. https://www.iea.org/reports/world-energy-outlook-2023. Accessed on 12 Jan 2024.

Xiao, W. (2017). *Photovoltaic power system: modeling, design, and control*. John Wiley & Sons.

Zhou, S., Kang, L., Sun, J., Guo, G., Cheng, B., Cao, B., and Tang, Y. (2010). A novel maximum power point tracking algorithms for stand-alone photovoltaic system. *International journal of control, automation and systems*, 8, 1364–1371.